Highly Improved Sb_2S_3 Sensitized-Inorganic–Organic Heterojunction Solar Cells and Quantification of Traps by Deep-Level Transient Spectroscopy

Yong Chan Choi, Dong Uk Lee, Jun Hong Noh, Eun Kyu Kim, and Sang Il Seok**

The light-harvesting Sb_2S_3 surface on mesoporous-TiO_2 in inorganic–organic heterojunction solar cells is sulfurized with thioacetamide (TA). The photovoltaic performances are compared before and after TA treatment, and the state of the Sb_2S_3 is investigated by X-ray diffraction, X-ray photoelectron spectroscopy, and deep-level transient spectroscopy (DLTS). Although there are no differences in crystallinity and composition, the TA-treated solar cells exhibit significantly enhanced performance compared to pristine Sb_2S_3-sensitized solar cells. From DLTS analysis, the performance enhancement is mainly attributed to the extinction of trap sites, which are present at a density of $(2–5) \times 10^{14}$ cm^{-3} in Sb_2S_3, by TA treatment. Through such a simple treatment, the cell records an overall power conversion efficiency (PCE) of 7.5% through a metal mask under simulated illumination (AM 1.5G, 100 mW cm^{-2}) with a very high open circuit voltage of 711.0 mV. This PCE is, thus far, the highest reported for fully solid-state chalcogenide-sensitized solar cells.

1. Introduction

The whole thrust of solar technology research and development is to produce high efficiency solar cells at low cost. Recently, metal chalcogenides, such as CdS(e),[1] PbS(e),[2] HgTe(e),[3] CuInTe(Se),[4] and $Sb_2S(e)_3$,[5] have attracted considerable attention because of their unique properties which include high absorption coefficient, intrinsic large dipole moment, convenient band gap tuning, the capacity for multiple excitations, and solution processibility. These properties increase their attractiveness as light sensitizers for applications in high-efficiency quantum dots and as extremely thin absorbers in sensitized solar cells. Among these compounds, Sb_2S_3 (stibnite) is particularly appealing as an efficient light absorber because of its suitable band gap (≈1.7 eV), strong absorption coefficient (1.8×10^5 cm^{-1} in the visible region), and relatively environmentally friendly characteristics.[6]

Intensive efforts have been exerted to improve the performance of solid-state Sb_2S_3-sensitized solar cells,[5a–h] since a power conversion efficiency (PCE) of 3.37% was recorded in solar cells employing CuSCN as a hole transporting material (HTM) by Itzhaik, et al.[5a] For example, poly(3-hexylthiophene) (P3HT) and poly(2,6-(4,4-bis-(2-ethylhexyl)-4*H*-cyclopenta[2,1-*b*;3,4-*b*′]dithiophene)-alt-4,7(2,1,3-benzothiadiazole)) (PCPDTBT) have been applied to the cells as effective organic HTMs.[5b–e] In addition, TiO_2 surfaces have been modified by decylphosphonic acid, Mg^{2+} ions, and Ba^{2+} ions to reduce recombination between the Sb_2S_3 and HTMs,[5c,g] and Ti, Zn, and Bi have been doped into the Sb_2S_3.[5h] Although we recently achieved a record PCE of 6.3% by incorporating electron channels from [6,6]-phenyl-C_{60}-butyric acid methyl ester (PCBM) in the low band gap PCPDTBT,[5e] the device performance was still low, as compared to that of solid-state dye-sensitized solar cells.[7] One factor responsible for the low PCE was the low open circuit voltage (V_{OC}), which mainly resulted from the recombination process in the Sb_2S_3.[8] Recently, the Kamat group showed that the presence of sulfide radical species in Sb_2S_3, which acted as hole trap sites, caused the slow extraction of holes compared to electrons, leading to increased recombination at the TiO_2/Sb_2S_3 interface.[9] Our recent studies based on a deep level transient spectroscopy (DLTS) revealed the trap sites for carrier recombination at the TiO_2/Sb_2S_3 interface in the Sb_2S_3.[10] The trap sites were positioned around E_C of –1.03 eV below the conduction band. Therefore, to improve device performance, surface defects (or electron/hole trap sites), which may act as recombination centers, should be significantly reduced.

In Sb_2S_3-sensitized solar cells, three factors may contribute to the surface defects in the Sb_2S_3. First, a sulfur-deficient phase (i.e., sulfur vacancies) can be readily formed in the Sb_2S_3 as a consequence of sulfur loss during the crystallization process.[11] Second, the oxidation of Sb_2S_3 quickly occurs

Dr. Y. C. Choi, Dr. J. H. Noh, Dr. S. I. Seok
Division of Advanced Materials
Korea Research Institute of Chemical Technology
141 Gajeong-Ro, Yuseong-Gu, Daejeon 305.600, Republic of Korea
Dr. D. U. Lee, Prof. E. K. Kim
Department of Physics and Quantum Function Research Laboratory
Hanyang University
Seoul 133–791, Republic of Korea
E-mail: ek-kim@hanyang.ac.kr
Prof. S. I. Seok
Department of Energy Science
Sungkyunkwan University
Seoul 440–746, Republic of Korea
E-mail: seoksi@skku.edu

DOI: 10.1002/adfm.201304238

at the surface upon exposure to air, which leads to the formation of surface oxides, such as Sb_2O_3 and sulfates.[12] During oxidation, some surfaces can be oxidized to form the oxides, resulting in defect formation on the surface. Third, the presence of impurities in Sb_2S_3 may cause the defects. In particular, the Sb_2S_3 synthesized by the water-based chemical bath deposition (CBD) method, a popular method used for solar cell preparation, inevitably includes some impurities, such as SbOCl, Sb_2O_3, and $Sb_2(SO_3)_3$.[13] In addition, the surface effects would be significant because of the high surface area-to-volume ratio, since the Sb_2S_3 generally exists in the form of quantum dots or extremely thin layers on the surface of the TiO_2 electrode in these solar cells. Thus, these characteristics make the surfaces prone to high trap state densities. Therefore, the surface treatment of Sb_2S_3 for the reduction of defect states is a key strategy to enhance device efficiency, particularly the V_{OC}.

Thioacetamide (TA) has been widely used as the sulfur source for the formation of metal sulfides because of its solution accessibility and high reactivity with metal ions.[13c,14] Compared to the popular sulfur source, Na_2S, TA can be dissolved in water-free organic solvents[13c] and produces pure sulfides.[14d,15] Furthermore, TA produces a highly reactive gas (H_2S) by thermal decomposition;[16] gaseous H_2S-based sulfurization has been widely used in $Cu(In,Ga)(S,Se)_2$ thin film solar cells to reduce the recombination centers through the controlled incorporation of sulfur.[17] Therefore, it is expected that the surface treatment of Sb_2S_3 with TA would provide a good platform for reducing the recombination centers in Sb_2S_3 without forming impurity phases on the surface.

In this work, we modified the surface of Sb_2S_3 by TA-based sulfurization. The process was conducted by spin-coating substrates with TA solutions followed by thermal annealing at 300 °C under Ar. X-ray photoelectron spectroscopy (XPS) and DLTS showed that the surface oxides were significantly reduced and the surface defects decreased after TA sulfurization. Sb_2S_3-sensitized cells after TA sulfurization exhibited the highest PCE ever observed of ≈7.5% as well as a high V_{OC} of 711 mV under air mass 1.5 global (AM1.5G) standard irradiation of 100 mW cm^{-2}. Note that we carefully controlled the annealing conditions, such as the annealing time and cooling conditions, to suppress the formation of crystalline Sb_2O_3. This crystalline material can be easily formed during annealing and its presence increases the series resistance, leading to a decrease in the device performance, especially the short circuit current density (J_{SC}).[12b,18]

2. Results and Discussion

Figure 1a illustrates the process for the Sb_2S_3 surface treatment with TA solutions in the Sb_2S_3-sensitized inorganic-organic heterojunction solar cells. Prior to the deposition of PCPDTBT for HTM, TA solutions diluted in *N*,*N*-dimethylformamide (DMF) were spin-coated on the Sb_2S_3/mesoporous TiO_2 (mp-TiO_2)/TiO_2 blocking layer (BL)/F-doped SnO_2 (FTO) substrate. Then, the samples were annealed at 200–300 °C under Ar atmosphere. To find appropriate conditions for the TA treatment, we explored the effects of the TA concentration, number of TA treatment cycles, and annealing conditions on the photovoltaic device performance (see Supporting Information Figures S1,S2, and Tables S1,S2). The optimum conditions were 0.01 g mL^{-1} TA concentration, 3000 rpm spin-coating, 60 s spinning time, and 300 °C annealing temperature. The current density–voltage (*J*–*V*) characteristics before and after applying TA in Sb_2S_3-sensitized solar cells were measured under illumination with a light intensity of 100 mW cm^{-2}. The corresponding solar cell parameters are summarized in **Table 1**. As shown in the Figure 1b, and Table 1 after the TA treatment, both J_{SC} and V_{OC} remarkably increased, from 15.2 mA cm^{-2} and 570.5 mV to 16.7 mA cm^{-2} and 645.7 mV, respectively. The fill factor (FF) was slightly increased. Eventually, the overall PCE was significantly improved from 5.5% to 7.1%. We also note that the dark current characteristics showed much lower dark currents in the device with TA treatment than the device without, as shown in Figure 1c, suggesting a decrease in the number of surface defects by TA treatment.

To elucidate the reasons behind the performance enhancement, we investigated the correlation between the structural changes and PCE improvement by measuring the X-ray diffraction (XRD) patterns of Sb_2S_3/mp-TiO_2/BL/FTO before and after treatment. In the XRD pattern of the sample without TA treatment (No TA, **Figure 2**), fifteen peaks (denoted by S) were observed without other impurity phases, such as Sb_2O_3. These peaks exactly matched orthorhombic Sb_2S_3 (JCPDS No. 42–1393). The pattern of the TA-treated sample (TA) was identical to that of the untreated sample (No TA). The Raman spectra were also identical, as the XRD patterns, in the vibrational states (Supporting Information Figure S3). These results implied that the structure was not changed upon TA treatment. Thus, it can be deduced that the efficiency enhancement by the TA treatment was not derived from structural changes of the Sb_2S_3.

To better understand the changes in the cell that resulted in the simultaneous improvements in the J_{SC}, V_{OC}, and FF values, we characterized and compared the Sb_2S_3 surface state by XPS before and after TA treatment. As shown in Supporting Information Figure S4, a peak difference for the Ti 2*p* spectra was not observed before or after TA treatment, implying there were no surface changes in the mp-TiO_2. In contrast, the spectra of Sb 3*d* and S 2*p* exhibited markedly different characteristics depending on the TA surface treatment. **Figure 3**a shows the high resolution XPS spectra of Sb $3d_{3/2}$. For the No TA sample, two peaks were observed at binding energies of 539.9 and 538.9 eV. These peaks could be indexed as Sb^{3+} oxidation states for Sb_2O_3 and Sb_2S_3, respectively.[12b,13c] This result indicated that the oxide, Sb_2O_3, was present on the surface of the Sb_2S_3; however, the absence of the Sb_2O_3 phase in the XRD pattern indicated (black pattern of Figure 2) that the Sb_2O_3 was not present in the crystalline form. By comparing the XPS peak area of Sb_2O_3 with that of Sb_2S_3, we could estimate the relative atomic ratio of the two phases. The measured ratio of Sb_2O_3/Sb_2S_3 obtained from the No TA sample was 49/51. After the TA surface treatment, the oxide phase was dramatically reduced, such that the Sb_2O_3/Sb_2S_3 ratio was 20/80. In the S 2*p* spectrum of the No TA sample, three peaks were observed at binding energies of 168.6, 162.4, and 161.2 eV. The blue peak at 168.6 eV can be indexed as oxidized sulfuror[19] and sulfates [$Sb_2(SO_4)_3$].[20] The other two peaks corresponded to S $2p_{1/2}$ and S $2p_{3/2}$ of the S^{2-} oxidation state of Sb_2S_3, respectively.[21] Similarly to the peak changes observed in Figure 3a, the oxidized peak in the S 2*p* spectrum of the sample was removed after TA-treatment.

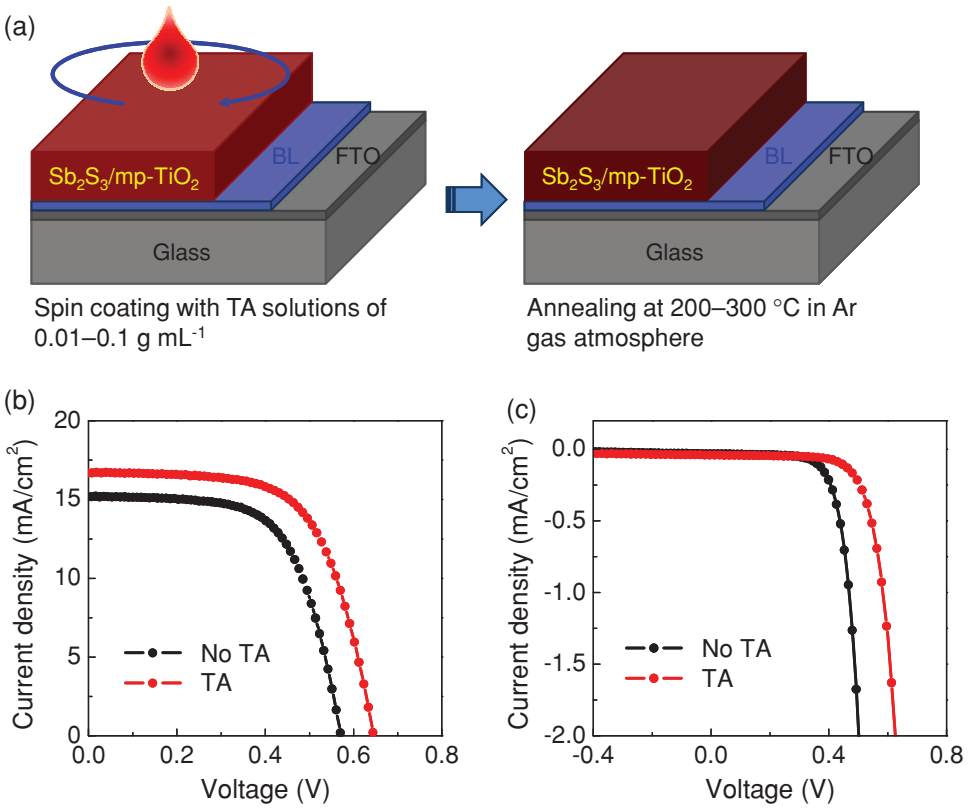

Figure 1. TA surface sulfurization and its effects on photovoltaic performance. a) Schematic diagram for the TA surface sulfurization process in the Sb_2S_3-sensitized inorganic-organic heterojunction solar cells. b) Effects of TA sulfurization on the *J–V* characteristics measured under AM 1.5G solar irradiance (100 mW cm^{-2}) and c) corresponding dark *J–V* curves. In (b,c), the devices with and without TA treatment are denoted as TA and No TA, respectively.

These results indicate that the TA treatment effectively reduces the oxide phases, such as Sb_2O_3 and oxidized sulfur, on the surface of Sb_2S_3. The decrease in the Sb_2O_3 phase can be attributed to its transformation to Sb_2S_3 during TA-treatment. Gaseous hydrogen sulfide is released by TA decomposition during annealing at 300 °C when the TA (CH_3CSNH_2) is decomposed into acetonitrile (CH_3CN) and hydrogen sulfide (H_2S) above 150 °C in an inert atmosphere.[16] Then, the released H_2S may readily react with the surface Sb_2O_3 to form Sb_2S_3, because the H_2S-assisted sulfurization of Sb_2O_3 is thermodynamically very favorable.[22] As a result, the Sb_2O_3 can be remarkably reduced after TA treatment, as revealed in Figure 3a. The possible chemical reactions for the transformation of Sb_2O_3 to Sb_2S_3 are described as follows:

$$CH_3CSNH_2 \rightarrow CH_3CN(g) + H_2S(g)$$

$$Sb_2O_3 + 3H_2S(g) \rightarrow Sb_2S_3 + 3H_2O(g)$$

Table 1. Photovoltaic parameters of devices shown in Figure 1b.

	J_{SC} [mA cm^{-2}]	V_{OC} [mV]	FF (%)	PCE (%)
No TA	15.2	570.5	64.0	5.5
TA	16.7	645.7	65.1	7.1
Improvement (%)	9.8	13.2	1.7	29.1

In case of the oxidized sulfur or sulfates, they may be released from the surface of Sb_2S_3 during the TA treatment. We believe that the reduction of the oxidized phases after TA

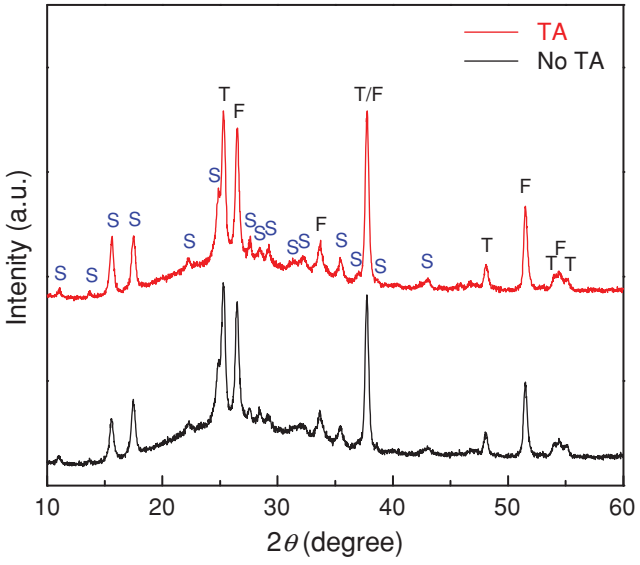

Figure 2. Effects of TA sulfurization on structure of Sb_2S_3. XRD patterns of Sb_2S_3/mp-TiO_2/BL/FTO with and without TA treatment, denoted as TA and No TA, respectively. S: Sb_2S_3; T: TiO_2; and F: FTO.

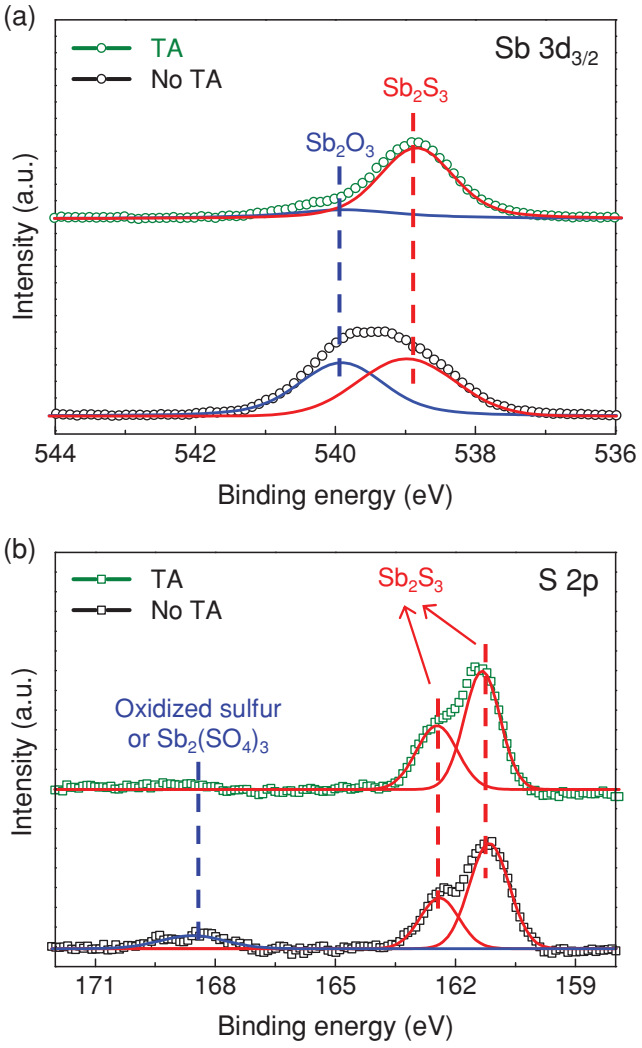

Figure 3. Effects of TA sulfurization on surface states of Sb_2S_3. High resolution XPS spectra of a) Sb $3d_{3/2}$ and b) S 2*p* of No TA and TA samples. Note that the peaks of Sb $3d_{5/2}$ located near 530 eV were excluded from the analysis because the peak for the O^{2-} state of TiO_2 overlapped those of the two Sb $3d_{5/2}$ peaks for Sb_2O_3 and Sb_2S_3.

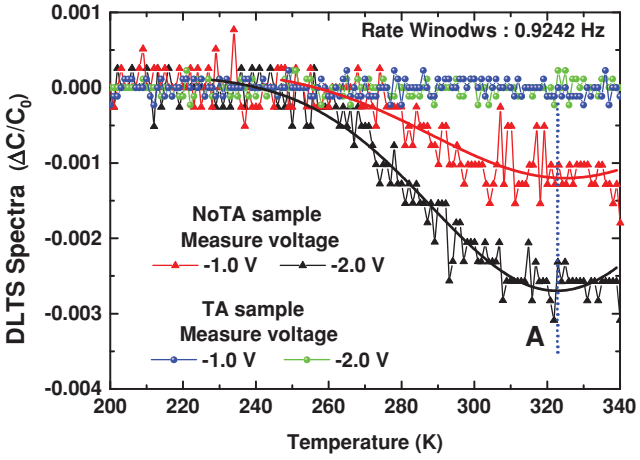

Figure 4. Effects of TA sulfurization on defect states of Sb_2S_3. Typical DLTS spectra of the Sb_2S_3 samples with and without TA treatment. Here, the measurements were done at a rate window of 0.9242 Hz under measurement voltages of –1.0 and –2.0 V after applying a pulse voltage of 0 V.

treatment also may contribute to the enhancement of the J_{SC}, as shown in Figure 1b and Table 1, because of the increased contribution of transformed Sb_2S_3 to the J_{SC}. Furthermore, the pure Sb_2S_3 may help to enhance the FF, because of the unique interaction between Sb_2S_3 and the bithiophene moieties of PCPDTBT as HTM.[5d]

To obtain physical insight into the population and distribution of the trap sites responsible for the overall performance of the cells, we investigated the defect states of Sb_2S_3 before and after TA treatment using DLTS. Recently, DLTS was successfully applied to quantify deep traps in nanocrystalline solids.[14c,23] **Figure 4** shows the DLTS spectra of the Sb_2S_3 samples before and after TA treatment. Schottky diodes using Au gate electrodes with 500 μm diameter were fabricated on the Sb_2S_3 samples for capacitance transient-based DLTS measurement.[24] Here, the measurements were performed in a rate window of 0.9242 Hz under the bias voltages of –1.0 V and –2.0 V after applying a pulse voltage of 0 V. As shown in Figure 4, the TA-treated sample did not produce any DLTS signal, whereas the untreated sample exhibits the signal A as a hole-like trap at all measurement voltages. The activation energy (E_v + 0.52 eV) and capture cross section (1.34×10^{-17} cm^2) of signal A were obtained by Arrhenius plot (method for detailed analysis was explained in Supporting Information with Figure S5); then, its origin was reported as a hole trap state in Sb_2S_3.[9] The defect density for signal A was estimated at about (2–5) $\times$ 10^{14} cm^{-3} from the signal intensities and carrier concentrations under the measurement bias voltages. Therefore, we suggest that the TA sulfurization process for Sb_2S_3 particles coated on an mp-TiO_2 layer transformed the Sb_2O_3 phase to Sb_2S_3, which may be caused by the sulfur passivation effect. Ultimately, the surface sulfurization of Sb_2S_3 enhanced the overall performance of the cells by reducing oxidized phases and the trap density.

Based on these effective strategies to improve the performance of Sb_2S_3-sensitized solar cells by TA treatment, we optimized and repeated the fabrication procedure by varying the Sb_2S_3 CBD reaction times from 2 h 10 min to 2 h 40 min and the concentrations of PCPDTBT in 1,2-dichlorobenzene. The PCE histograms of each individually fabricated device revealed that the TA-treated devices had an average PCE that was ~5.5%, higher than that of the No TA devices (≈4.7%, **Figure 5**a). These results indicate that the TA surface treatment obviously contributed to the improvement in the device performance by the remarkable increases in J_{SC} and V_{OC}. The most efficient devices were obtained after 2 h 20–25 min CBD and at 10 mg mL^{-1} PCPDTBT. As shown in Figure 5b and **Table 2**, the champion device exhibited a PCE of ≈7.5%, with a J_{SC} of 16.1 mA cm^{-2}, V_{OC} of 711.0 mV, and FF of 65.0%, under AM1.5G illumination with an intensity of 100 mW cm^{-2}. At low light intensities of 10 and 50 mW cm^{-2}, the PCE values were 8.4% and 8.7%, respectively. To the best of our knowledge, these are the highest PCEs as well as the highest V_{OC} values reported thus far for metal-chalcogenide-sensitized solid-state solar cells. The J_{SC} value of 15.9 mA cm^{-2}, obtained by integrating the incident

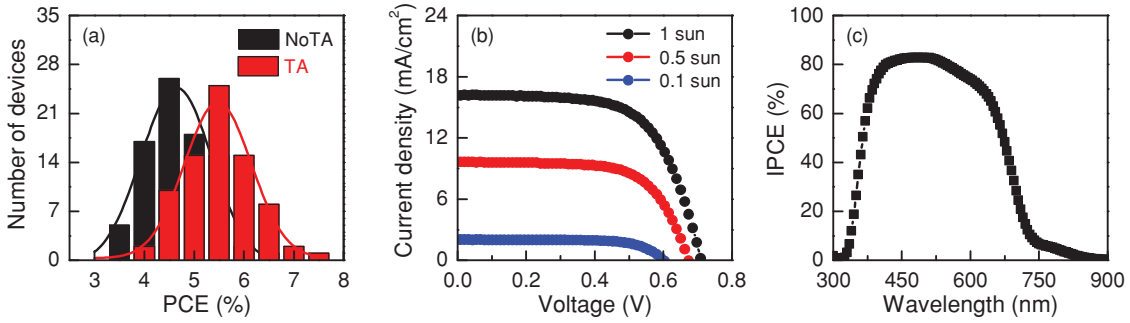

Figure 5. Photovoltaic performances of the champion device. a) Histograms of device efficiencies for identically fabricated cells. b) *J–V* characteristics and c) IPCE spectrum of the champion cell.

photon-to-current efficiency (IPCE) data (Figure 5c) with the AM 1.5G reference spectrum, was very close to that obtained using the *J–V* measurement.

3. Conclusions

In summary, we demonstrated an efficiency enhancement by the surface sulfurization of Sb_2S_3 in Au/PCPDTBT/Sb_2S_3/mp-TiO_2 inorganic-organic heterojunction solar cells. The surface sulfurization of Sb_2S_3 as light harvester was performed by spin-coating of TA, followed by thermal annealing at 300 °C for 1 min under Ar prior to the PCPDTBT deposition. DLTS showed that the defects with the density of (2–5) × 10^{14} cm^{-3} in Sb_2S_3 could be removed by TA treatment. Thus, it was considered that the performance enhancement could mainly be attributed to the reduction of trap sites in Sb_2S_3 by surface sulfurization. The best cell showed the highest V_{OC} of 711.0 mV and PCEs of 7.5, 8.7, and 8.4% at 100, 50, and 10% solar irradiation, respectively, with a metal mask. This work provides a simple method to improve the PCEs of inorganic semiconductor-sensitized solar cells.

4. Experimental Section

Solar Cell Fabrication: A thin TiO_2 BL of ca. 70-nm thickness was deposited on a cleaned FTO (Pilkington, TEC8, 8 Ω cm^{-2}) glass substrate by spray pyrolysis deposition with 20 mM titanium diisopropoxide bis(acetylacetonate) (Aldrich) solution at 450 °C. The TiO_2 paste containing TiO_2 nanoparticles (mp-TiO_2, average diameter 50 nm, anatase) was then screen-printed onto the BL/FTO substrate to a thickness of ≈ 1.3 µm, and the formed film was calcined at 500 °C for 1 h in air. The mp-TiO_2 film was then dipped into a 40 mM $TiCl_4$ aqueous solution at 60 °C for 1 h and washed with deionized water and sintered again at 500 °C for 30 min for intimate contact between the nanocrystalline TiO_2 particles. The Sb_2S_3 was deposited on the mp-TiO_2 film by CBD in a temperature controlled chiller and then heat-treated at 300 °C in an Ar atmosphere for 5 min. For the TA surface sulfurization, the TA solutions diluted in DMF (0.01–0.1 g mL^{-1}) were first synthesized at ambient conditions. The DMF solvent was dropped on the Sb_2S_3/mp-TiO_2/BL/FTO, and spin coated at 2000 rpm for 60 s for the efficient penetration of TA solutions into the pores of mp-TiO_2. Then, the TA solutions were spin coated on DMF-treated Sb_2S_3/mp-TiO_2/BL/FTO at the same condition as that for DMF-spin-coating. Afterwards, the samples were annealed at 200–300 °C in an Ar atmosphere for 1 min. For device fabrication, PCPDTBT solutions (5–15 mg mL^{-1} in 1,2-dichlorobenzene) were spin-coated onto Sb_2S_3/mp-TiO_2/BL/FTO film at 2000 rpm for 60 s. Then, poly(3,4-ethylenedioxythiophene) doped with poly(4-styrenesulfonate) (PEDOT:PSS; Baytron AI 4083), diluted threefold in MeOH, was spin-coated onto the PCPDTBT/Sb_2S_3/mp-TiO_2 film at 2000 rpm for 60 s. The PEDOT:PSS/PCPDTBT/Sb_2S_3/mp-TiO_2 was then dried at 90 °C for 30 min in a vacuum oven, and the Au counter electrode was finally deposited by a thermal evaporator under a pressure of 5 × 10^{-6} Torr. The active area of the device was fixed at 16 mm^2.

Characterization: The structure and surface state were characterized by XRD (Rigaku D/Max II X-ray dffractometer) and XPS (Thermo VG Scientific, Sigma Probe), respectively. All XPS binding energies were calibrated with the C–C peak at 284.6 eV in the C 1*s* spectra. The Raman spectra were obtained by using the excitation wavelength of 514.5 nm (Ar ion laser). The absorption spectra were measured using a UV-Vis spectrometer (Shimadzu UV-2600). The DLTS spectra were measured using an automatic computer controlled system consisted with a HP4280A 1-MHz capacitance meter, a Boonton 7200 1-MHz capacitance meters, a HP8116A pulse function generator 50 MHz, a SR 640 dual-channel low-pass filter, a data acquisition system, a Lakeshare 331 temperature controller, a cryostat (12–700 K), and a DLTS Labview program. The diameter and thickness of Au electrode on Sb_2S_3 layer for Schottky contact were 500 µm and 200 nm, respectively. To improve the resolution of DLTS spectra, the tolerance of measuring temperature was 0.01 K by using the auto-proportional-integral-differential control of Lakeshare 331 temperature control. The capacitance transient was analysed with time interval of 50 ms after applying 0-V-bias pulse with pulsed width of 15 ms under a reverse bias, and it was carried out three times at a temperature and averaged to define DLTS spectra. The *J–V* curves were measured with a metal mask 0.1225 cm^2 in area using a solar simulator (Newport, Oriel Class A, 91195A) with a source meter (Keithley 2400) at 100 mA cm^{-2} illumination AM 1.5G and a calibrated Si-reference cell certificated by NREL. The IPCE spectra were measured using a power source (Newport 300 W Xenon lamp, 66920) with a monochromoto (Newport Cornerstone 260) and a multimeter (Keithley 2001).

Table 2. Photovoltaic parameters of champion device shown in Figure 5b.

Light power [mW cm^{-2}]	J_{SC} [mA cm^{-2}]	V_{OC} [mV]	FF (%)	PCE (%)
100	16.1	711.0	65.0	7.5
50	9.6	672.7	67.0	8.7
10	2.0	600.1	70.0	8.4

Supporting Information

Supporting Information is available from the Wiley Online Library or from the author.

Acknowledgements

Y.C.C. and D.U.L. contributed equally to this work. This study was supported by the Global Research Laboratory (GRL) Program and the Global Frontier R&D Program on Center for Multiscale Energy System funded by the National Research Foundation under the Ministry of Science, ICT & Future, Korea, and by a grant from the KRICT 2020 Program for Future Technology of the Korea Research Institute of Chemical Technology (KRICT), Republic of Korea.

Received: December 20, 2013
Revised: January 19, 2014
Published online: March 3, 2014

[1] a) Y. L. Lee, Y. S. Lo, *Adv. Funct. Mater.* **2009**, *19*, 604; b) Y. H. Lee, S. H. Im, J. H. Rhee, J.-H. Lee, S. I. Seok, *ACS Appl. Mater. Interfaces* **2010**, *2*, 1648; c) P. V. Kamat, *Acc. Chem. Res.* **2012**, *45*, 1906; d) S. H. Im, Y. H. Lee, S. I. Seok, *Electrochim. Acta* **2010**, *55*, 5665; e) T. Zeng, H. Tao, X. Sui, X. Zhou, X. Zhao, *Chem. Phys. Lett.* **2011**, *508*, 130; f) Y. H. Lee, S. H. Im, J. A. Chang, J.-H. Lee, S. I. Seok, *Org. Electron.* **2012**, *13*, 975.

[2] a) S. Kim, S. H. Im, M. Kang, J. H. Heo, S. I. Seok, S.-W. Kim, I. Mora-Sero, J. Bisquert, *J. Phys. Chem. Chem. Phys.* **2012**, *14*, 14999; b) N. Guijarro, T. Lana-Villarreal, T. Lutz, S. A. Haque, R. Gomez, *J. Phys. Chem. Lett.* **2012**, *3*, 3367; c) S. H. Im, H. Kim, S. Kim, S.-W. Kim, S. I. Seok, *Org. Electron.* **2012**, *13*, 2352; d) S. H. Im, S. H. Kim, S. W. Kim, S.-W. Kim, S. I. Seok, *Energy Environ. Sci.* **2011**, *4*, 4181; e) N. P. Benehkohal, V. Gonzalez-Pedro, P. P. Boix, S. Chavhan, R. Tena-Zaera, G. P. Demopoulos, I. Mora-Sero, *J. Phys. Chem. C* **2012**, *116*, 16391.

[3] a) S. Kim, T. Kim, S. H. Im, S. I. Seok, K. W. Kim, S. Kim, S.-W. Kim, *J. Mater. Chem.* **2011**, *21*, 15232; b) S. H. Im, H. Kim, S. Kim, S.-W. Kim, S. I. Seok, *Nanoscale* **2012**, *4*, 1581.

[4] S. Kim, M. Kang, S. Kim, J.-H. Heo, J. H. Noh, S. H. Im, S. I. Seok, S.-W. Kim, *ACS Nano* **2013**, *7*, 4756.

[5] a) Y. Itzhaik, O. Niitsoo, M. Page, G. Hodes, *J. Phys. Chem. C* **2009**, *113*, 4254; b) S.-J. Moon, Y. Itzhaik, J.-H. Yum, S. M. Zakeeruddin, G. Hodes, M. Gratzel, *J. Phys. Chem. Lett.* **2010**, *1*, 1524; c) J. A. Chang, J. H. Rhee, S. H. Im, Y. H. Lee, H.-J. Kim, S. I. Seok, *Nano. Lett.* **2010**, *10*, 2609; d) S. H. Im, C.-S. Lim, J. A. Chang, Y. H. Lee, N. Maiti, H.-J. Kim, Md. K. Nazeeruddin, M. Gratzel, S. I. Seok, *Nano. Lett.* **2011**, *11*, 4789; e) J. A. Chang, S. H. Im, Y. H. Lee, H.-J. Kim, C.-S. Lim, J. H. Heo, S. I. Seok, *Nano. Lett.* **2012**, *12*, 1863; f) Y. H. Lee, J. H. Heo, S. H. Im, H.-J. Kim, C.-S. Lim, T. K. Ahn, S. I. Seok, *Chem. Phys. Lett.* **2013**, *3*, 29; g) K. Tsujimoto, D.-C. Nguyen, S. Ito, H. Nishino, H. Matsuyoshi, A. Konno, G. R. A. Kumara, K. Tennakone, *J. Phys. Chem. C* **2012**, *116*, 13465; h) S. Ito, K. Tsujimoto, D.-C. Nguyen, K. Manabe, H. Nishino, *Int. J. Hydrogen Energy* **2013**, *38*, 16749; i) Y. C. Choi, T. N. Mandal, W. S. Yang, Y. H. Lee, S. H. Im, J. H. Noh, S. I. Seok, *Angew. Chem. Int. Ed.* **2014**, *53*, 1329.

[6] M. Y. Versavel, J. A. Haber, *Thin Solid Films* **2007**, *515*, 7171.

[7] I. Chung, B. Lee, J. He, R. P. H. Chang, M. G. Kanatzidis, *Nature* **2012**, *485*, 486.

[8] a) P. P. Boix, G. Larramona, A. Jacob, B. Delatouche, I. Mora-Sero, J. Bisquert, *J. Phys. Chem. C* **2012**, *116*, 1579; b) P. P. Boix, Y. H. Lee, F. Fabregat-Santiago, I. Mora-Sero, J. Bisquert, S. I. Seok, *ACS Nano* **2012**, *6*, 873.

[9] J. A. Christians, P. V. Kamat, *ACS Nano* **2013**, *7*, 7967.

[10] D. U. Lee, S. W. Park, S. G. Cho, E. K. Kim, S. I. Seok, *Appl. Phys. Lett.* **2013**, *103*, 023901.

[11] a) P. Arun, A. G. Vedeshwar, *J. Appl. Phys.* **1996**, *79*, 4029; b) F. Perales, G. Lifante, F. Agullo-Rueda, C. D. L. Heras, *J. Phys. D: Appl. Phys.* **2007**, *40*, 2440.

[12] a) V. P. Zakaznova-Herzog, S. L. Harmer, H. W. Nesbitt, G. M. Bancroft, R. Flemming, A. R. Pratt, *Surf. Sci.* **2006**, *600*, 348; b) B. Reeja-Jayan, A. Manthiram, *RSC Adv.* **2013**, *3*, 5412.

[13] a) C. D. Lokhande, B. R. Sankapal, R. S. Mane, H. M. Pathan, M. Muller, M. Giersig, V. Ganesan, *Appl. Surf. Sci.* **2002**, *193*, 1; b) S. M. Pawar, B. S. Pawar, J. H. Kim, O.-S. Joo, C. Lokhande, *Curr. Appl. Phys.* **2011**, *11*, 117; c) N. Maiti, S. H. Im, C.-S. Lim, S. I. Seok, *Dalton Trans.* **2012**, *41*, 11569.

[14] a) H. Su, Y. Xie, P. Gao, Y. Xiong, Y. Qian, *J. Mater. Chem.* **2001**, *11*, 684; b) M. W. Xiao, L. Wang, Y. Wu, X. Huang, Z. Dang, *Nanotechnology* **2008**, *19*, 015706; c) D.-R. Jung, D. Son, J. Kim, C. Kim, B. Park, *Appl. Phys. Lett.* **2008**, *93*, 163118; d) S. H. Liu, X. F. Qian, J. Yin, H. A. Xi, Z. H. Huang, Z. K. Zhu, *Mater. Sci. Eng. B* **2003**, *B98*, 99.

[15] P. Patnaik, *Handbook of Inorganic Chemicals* **2002**, New York, McGraw-Hill.

[16] S. Bent, J. S. King, J. R. Bakke, Process for in situ generation of hydrogen sulfide or hydrogen selenide gas using a solid precursor. *EP 2 199 257 A2*, June 23, **2010**.

[17] N. G. Dhere, *Sol. Energy Mater. Sol. Cells* **2006**, *90*, 2181.

[18] Ee L. Gui, A. M. Kang, S. S. Pramana, N. Yantara, N. Mathews, S. Mhaisalkar, *J. Electrochem. Soc.* **2012**, *159*, B247.

[19] X. Wang, W. Hu, R. Ramasubramaniam, G. H. Bernstein, G. Snider, M. Lieberman, *Langmuir* **2003**, *19*, 9748.

[20] a) R. Bayon, C. Maffiotte, J. Herrero, *Thin Solid Films* **1999**, *353*, 100; b) H. El Maliki, J. C. Bernede, S. Marsillac, J. Pinel, X. Castel, J. Pouzet, *Appl. Surf. Sci.* **2003**, *205*, 65.

[21] K. Xiao, Q.-Z. Xu, K.-H. Ye, Z.-Q. Liu, L.-M. Fu, N. Li, Y.-B. Chen, Y. Z. Su, *ECS Solid State Lett.* **2013**, *2*, P51.

[22] B. H. Juarez, M. Ibisate, J. M. Palacios, C. Lopez, *Adv. Mater.* **2003**, *15*, 319.

[23] a) D. Bozyigit, M. Jakob, O. Yarema, V. Wood, *ACS Appl. Mater. Interfaces* **2013**, *5*, 2915; b) D. Bozyigit, S. Volk, M. Jakob, O. Yarema, V. Wood, *Nano Lett.* **2013**, *13*, 5284.

[24] J. P. Clifford, K. W. Johnston, L. Levina, E. H. Sargent, *Appl. Phys. Lett.* **2007**, *91*, 253117.